International Journal of Computational Fluid Dynamics, 2002 VOL. 16 (3), pp. 217–227

Taylor & Francis
Taylor & Francis Group

Calculation of Ship Sinkage and Trim Using a Finite Element Method and Unstructured Grids

CHI YANG and RAINALD LÖHNER*

School of Computational Sciences, George Mason University, M.S. 4C7, 4400 University Drive, Fairfax, VA 22030-4444, USA

(Received 12 October 2000; Revised 20 February 2001; In final form 13 March 2001)

An unstructured grid-based, parallel free-surface flow solver has been extended to account for sinkage and trim effects in the calculation of steady ship waves. The overall scheme of the solver combines a finite-element, equal-order, projection-type three-dimensional incompressible flow solver with a finite element, two-dimensional advection equation solver for the free surface equation. The sinkage and trim, wave profiles, and wave drag computed using the present approach are in good agreement with experimental measurements for two hull forms at a wide range of Froude numbers. Numerical predictions indicate significant differences between the wave drag for a ship fixed in at-rest position and free to sink and trim, in agreement with experimental observations.

Keywords: Finite elements; Unstructured grids; Free surface; Ship hydrodynamics; Finite element method

1. INTRODUCTION

A steadily advancing surface ship experiences sinkage and trim, notably at high Froude numbers, due to the hydrodynamic forces acting on the ship hull. Sinkage and trim effects are also observed in towing tank experiments if the ship model is not fixed to the towing carriage. A ship model free to sink and trim can experience an increase in wave resistance. Large trim changes may also affect the performance of a ship. For example, bow-down trim affects the taking off of airplanes from a carrier. Sinkage and trim in very shallow water may set an upper limit to the speed at which ships can operate without touching bottom. Therefore, it is of practical importance to include sinkage and trim effects in the calculation of steady ship waves.

In recent years, the advent of advanced numerical schemes for the Euler and Navier–Stokes equations has enabled more realistic predictions of wave resistance. In these schemes, a three-dimensional, i.e. a volumetric incompressible flow solver, is coupled with a free surface equation given by the kinematic boundary condition. The velocities obtained at the free surface from the three-dimensional incompressible flow solver are used in the free surface solver to update the free surface height. This new height changes the (prescribed) pressure at the free surface for the three-dimensional incompressible flow solver, thereby closing the loop. The free surface height also serves as the basis for the mesh motion.

There exist two main types of incompressible flow solvers. The first class is based on projection schemes (Chorin, 1968; Kim and Moin, 1985; Hino, 1989; Martin and Löhner, 1992; Luo *et al.*, 1995; Alessandrini and Delhommeau, 1996; Kallinderis and Chen, 1996; Miyata, 1996; Ramamurti and Löhner, 1996; Löhner *et al.*, 1998; 1999; Yang and Löhner, 1998; Yang *et al.*, 1999). A velocity field is predicted in a first step. The conservation of mass is enforced in a second step by solving a Poisson equation, which results in a new pressure. Finally, the velocity field is updated using this new pressure. The second class is based on artificial compressibility schemes (Chorin, 1967; Rizzi and Eriksson, 1985; Farmer *et al.*, 1993; Hino *et al.*, 1993; Haussling and Miller, 1994; Martinelli and Farmer, 1994; Peraire *et al.*, 1994; Cowles and Martinelli, 1996; 1998; Haussling *et al.*, 1997; Hino, 1997; 1998). The infinite speed of sound of the incompressible medium is reduced to a finite number by adding a time derivative of the pressure to the divergence equation. This approach enables the effective use of all the techniques developed for compressible flow simulation, such as limitors, upwind differencing, residual smoothing, multigrid acceleration, etc. At steady state, the time

*Corresponding author.

ISSN 1061-8562 print/ISSN 1029-0257 online © 2002 Taylor & Francis Ltd
DOI: 10.1080/10618560290034690

derivative in the divergence equation vanishes, yielding the proper incompressible solution. Both families of solvers have been used successfully to develop computer codes for free-surface prediction, including total ship resistance or wave resistance. However, most calculations so far consider the case in which the ship is fixed at either the at-rest position or a prescribed sunk and trimmed position given by model tests.

Due to the significant effects of sinkage and trim on resistance and performance, dynamic sinkage and trim should be incorporated in calculations of steady ship waves. Consideration of sinkage and trim also provides a better way of validating resistance data since many experiments are performed for ship models free to sink and trim. The general objective of this work is therefore the development of a more efficient method to predict steady ship waves while taking sinkage and trim into account.

During the last 3 years, an unstructured grid-based, parallel free-surface flow solver has been developed for solving nonlinear ship-wave-resistance problems in terms of the Euler or Reynolds-averaged Navier Stokes (RANS) formulation for the case in which the ship is fixed (Löhner *et al.*, 1998; 1999; Yang and Löhner, 1998; Yang *et al.*, 1999). The overall scheme combines a finite-element, equal-order, projection-type three-dimensional incompressible flow solver with a finite element, two-dimensional advection equation solver for the free surface equation. This free-surface flow solver is extended in the present paper to incorporate dynamic sinkage and trim in the steady wave calculation. As the first step of the study, the Euler formulation is employed here. The solution procedure consists of the following steps.

(1) A steady flow simulation is performed for the case in which the ship is fixed at the initial at-rest position.
(2) The ship model is then moved to a predicted sunk and trimmed position. The grids on the hull and in the vicinity of the hull are rigidized during the hull movement.
(3) A steady flow simulation is performed again while the hull is fixed at the predicted sunk and trimmed position. A converged free surface is obtained at the end of the present step for this ship model position.

The second and third steps are repeated until a converged sunk and trimmed position is reached, i.e. all the forces and moments that act upon the ship model are in equilibrium. The solution from the previous iteration serves as the initial condition to speed up the steady flow simulation.

An unstructured grid is used in the present finite element method to enhance geometry flexibility and to speed up the initial modeling time. Specifically, a triangulation is first generated directly from the offset data. This triangulation is subsequently used to define the hull surface in a discrete manner. The surface definition of the complete computational domain consists of discrete (hull) and analytical surface patches. An automatic unstructured grid generator based on the advancing front method is used to generate triangular surface grids and tetrahedral volume grids. In addition, the unstructured grid generator is linked to the flow solver, so that an automatic remeshing can easily be performed to simulate fully nonlinear ship waves.

The present paper is organized as follows: The second section summarizes the equations used to describe the flow and free surface, and the solution procedure of the Euler solver; third section describes the approach used for evaluating sinkage and trim; fourth section gives a brief review of some numerical aspects, including the techniques used in unstructured grid generation and mesh update; some examples are shown in the fifth section; finally, some conclusions are given in the sixth section.

2. EULER SOLVER

Figure 1 shows the reference frame and ship model location used in the paper. A Cartesian coordinate system $Oxyz$ is fixed to the ship model with the origin inside the hull on the mean free surface. The z direction is positive upwards, y is positive towards the starboard side and x is positive in the aft direction. The free stream velocity vector is parallel to the x axis and points in the same direction.

2.1. Flowfield Equations

The equations solved are the incompressible Euler equations given, in nondimensional form, by the conservation of mass and momentum:

$$\nabla\cdot\mathbf{v} = 0, \tag{1}$$

$$\mathbf{v}_{,t} + \mathbf{v}\cdot\nabla\mathbf{v} + \nabla\Psi = 0, \tag{2}$$

where $\mathbf{v} = (u, v, w)$ denotes the velocity vector and Ψ the

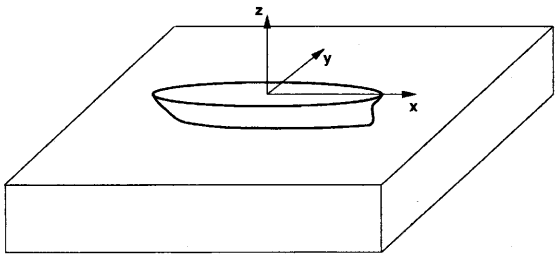

FIGURE 1 Coordinate system used.

pressure plus hydrostatic pressure:

$$\Psi = p + \frac{z}{Fr^2}, \quad Fr = \frac{|\mathbf{v}_\infty|}{\sqrt{g \cdot L}}. \tag{3}$$

A particle on the free surface must remain there, which implies that the free surface elevation β obeys the advection equation

$$\beta_{,t} + u\beta_{,x} + v\beta_{,y} = w. \tag{4}$$

The boundary conditions are as follows:

(a) *Inflow plane*: At the inflow plane, the velocity, pressure and free surface height are prescribed:

$$\mathbf{v} = (1, 0, 0), \quad \Psi = 0, \quad \beta = 0. \tag{5}$$

(b) *Exit plane*: At the exit plane, none of the quantities are prescribed. The natural Neumann condition for the pressure and extrapolation boundary conditions for the velocities and free surface height are imposed automatically by the numerical scheme used.

(c) *Free surface*: At the free surface, the pressure p is prescribed as $p = 0$, implying that Ψ is given by

$$\Psi = \beta Fr^{-2}. \tag{6}$$

Note that the kinematic free surface boundary condition is given by Eq. (4).

(d) *Bottom*: At the bottom, one may either impose the boundary condition for a
- *Wall*: vanishing normal velocity, Neumann condition for the pressure, or
- *Infinite Depth:* prescribed pressure, no boundary conditions for the velocities.

(e) *Ship hull*: On the ship hull, the normal velocity must vanish, i.e.

$$\mathbf{v} \cdot \mathbf{n} = 0, \tag{7}$$

where $\mathbf{n}$ is the normal to the hull.

(f) *Side walls*: On the side walls of the computational domain, we impose the same conditions as for the hull, i.e. vanishing normal velocity.

2.2. Solution Procedure

For the solution of the three-dimensional incompressible flow equations, a pressure projection scheme is used. The free surface Eq. (4) is treated as a standard scalar advection equation with source terms for the x, y plane. One complete timestep of the Euler solver consists of the following steps:

(1) Given the boundary conditions for the pressure Ψ, update the solution in the three-dimensional fluid mesh (velocities and pressures);
(2) Extract the velocity vector $\mathbf{v} = (u, v, w)$ at the free surface and transfer it to the two-dimensional free surface module;
(3) Given the velocity field, update the free surface β;
(4) Transfer back the new free surface β to the three-dimensional fluid mesh, and impose new boundary conditions for the pressure Ψ.

For steady-state applications, the fluid and free surface domains are updated using local timesteps. This allows some room for variants that may converge faster to the final solution, e.g. n steps of the fluid followed by m steps of the free surface, complete convergence of the free surface between fluid updates, etc. Our preference for steady-state applications is to use an equivalent "time-interval" ratio between fluid and free surface of 1:8, e.g. a Courant-nr. of $C_f = 0.25$ for the fluid and $C_s = 2.0$ for the free surface.

The formulation of the numerical procedure is based on a three-dimensional finite element method for the flow variables (u, v, w, ψ), coupled to a two-dimensional finite element method for the free surface evolution variable (β). The computational domain is represented by an unstructured assembly of four-noded tetrahedral elements. The faces on the free surface are extracted from the three-dimensional mesh and renumbered locally to obtain a two-dimensional triangular finite element mesh in x, y. A detailed description of the numerical solution procedure can be found in authors' previous work (Löhner *et al.*, 1998; 1999; Yang and Löhner, 1998; Yang *et al.*, 1999).

The Euler solver has been optimized for efficient use of parallel computer hardware. The solver allow steady wave predictions for a fixed hull model using approximately half a million tetrahedral element in less than an hour on widely available machines, e.g. the SGI Origin 2000 with four processors.

3. EVALUATION OF SINKAGE AND TRIM

The procedure used to compute sinkage and trim is now summarized.

(1) The hull model is first considered in its at-rest position. An automatic unstructured grid generator based on the advancing front technique is used to generate a surface mesh and a volume mesh. The x-coordinate of the center of gravity is determined from static equilibrium. A steady flow simulation is performed with the hull in this initial position.
(2) The net heave force and trim moment acting on the hull are calculated from the previous converged solution. The sinkage and trim corrections required by the equilibrium of this force and moment are evaluated. The hull model is repositioned and the grids are moved accordingly. Specifically, three

types of grid movements are considered. One type consists of the grids on the hull and in the vicinity of the hull. These near-field grids are moved rigidly with the hull. Another type consists of the grids far away from the hull. These far-field grids are not moved. Finally, the third type of grids consists of the remainder of the grids. These intermediate grids are moved smoothly in order to minimize mesh distortions (Löhner and Yang, 1996).

(3) A steady flow simulation is performed again while the hull model is fixed at the predicted sunk and trimmed position. A converged free surface is obtained for this given hull-model position at the end of the present step. The solution from the previous iteration is used as the initial condition to speed up the steady flow simulation.

The second and third steps are repeated until a converged sunk and trimmed position is obtained, i.e. until the net heave force and trim moment vanish.

The sinkage and trim corrections are expressed in terms of the net heave force and trim moment using the relations

$$\Delta H = \frac{L}{\rho g A_0^w}, \tag{8}$$

$$\Delta \alpha = \frac{M}{\rho g A_2^w}. \tag{9}$$

Here ΔH is the correction of the sinkage at the center of gravity, $\Delta\alpha$ is the trim angle correction, L and M are the net heave force and trim moment. A_0^w is the waterplane area, and A_2^w is the corresponding moment of inertia about the y axis. The heave force and trim moment are defined in terms of the pressure p, which is obtained explicitly in the Euler solver. The pressure is assumed to be constant within each triangular face on the hull in the pressure integration since the mesh on the hull is very fine.

4. NUMERICAL ASPECTS

4.1. Unstructured Grid Generation

The discretization of a general three-dimensional computational domain into an unstructured assembly of tetrahedra is accomplished by means of an advancing front grid generation procedure (Löhner, 1997). This procedure requires that the geometry of the computational domain be defined in terms of an assembly of surface patches, and that the spatial variation of element size and shape be prescribed. The first step in the process is the triangulation of the computational boundary surfaces. The assembly of resulting triangles forms the initial front for the three-dimensional grid generation process. The advancing front method is then used to fill the computational domain with tetrahedra, which are generated so as to meet a user-prescribed distribution of element size and shape.

Both analytical surface patches (planes, Coon's patches, etc.) and discrete surface patches (defined by a surface triangulation) are used to describe the present computational domain boundaries, which consist of the hull surface, free surface, inflow plane, exit plane and bottom plane. Specifically, the preprocessor FECAD first reads in the hull offset data. A triangulation is then generated from the offset data. This triangulation is subsequently used to define the hull surface in a discrete manner. The rest of the boundary surfaces are defined analytically.

The desired element size and shape are prescribed via background grids and sources. The computational domain is covered by a coarse background grid of tetrahedral elements. The desired element size and shape are then specified at the nodes of this background grid. During grid generation, the local element size and shape are obtained using linear interpolation. In addition, both line and surface sources are used on the hull surface and the free surface to further define the element size. The sources on the hull surface ensure the generation of a finer mesh to accurately capture the hull geometry and the complex flow in the bow and stern regions. The sources on the free surface yield a finer mesh in the Kelvin wave pattern region.

4.2. Mesh Update Procedure

Previous work by Farmer *et al.* (1993), Hino *et al.* (1993), and Hino (1997) marched the solution in time until steady state was reached. At each timestep, a volume update was followed by a free surface update. The repositioning of points at each timestep implies a complete recalculation of geometrical parameters, and interrogation of the CAD information defining the surface. In our case, this approach would double CPU requirements. For this reason, when solving steady-state problems, we do not move the grid at each timestep, but only change the pressure boundary condition after each update of the free surface β.

An initial steady-flow solution is first obtained without moving the grid. A predicted free surface elevation is then used to define the intersection curve of the free surface with the hull and the symmetry plane $y = 0$. Next, the free surface is updated using the previously-computed intersection curve, and a corresponding updated mesh is generated. A steady flow calculation is again performed using the new mesh, first without moving the grids and subsequently updating the mesh every 100–250 timesteps. This procedure ensures minimum mesh movements and thereby minimizes the costs associated with geometry recalculations and grid repositioning along surfaces. One mesh update consists of the following steps:

- Obtain the new elevation for the points on the free surface from β. This only results in a vertical (z-direction) displacement field $\mathbf{d}_\Gamma$ for the boundary points.
- Apply the proper boundary conditions for the points on the waterline. This results in an additional

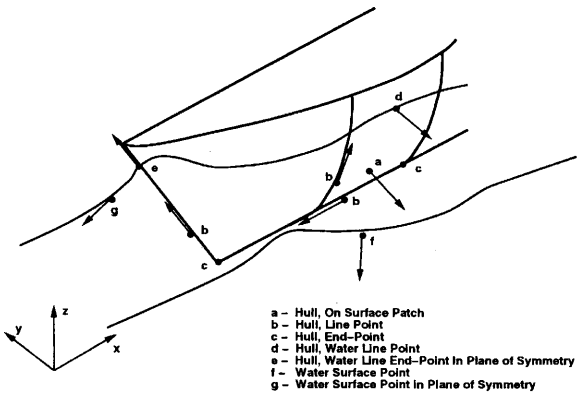

FIGURE 2 Boundary conditions for mesh movement.

horizontal (x, y-direction) displacement field for the points on the water line.

- Smooth the displacement field in order to avoid mesh distortion. The smoother used is of the form (Löhner and Yang, 1996):

$$\nabla \cdot k \nabla \mathbf{d} = 0, \tag{10}$$

where k is a nonlinear stiffness coefficient that depends on the distance from the hull.

- Interrogate the CAD data to reposition the points on the hull.

Figure 2 shows schematically the mesh movement boundary conditions that have to be taken into account (Löhner *et al.*, 1998; 1999).

Should negative elements arise due to surface point repositioning, they are removed and a local remeshing takes place. Naturally, these situations should be avoided as much as possible.

4.3. Addition of Sinkage and Trim

As explained in the third section, the hull model is repositioned in accordance with the net heave force and trim moment acting on the hull. This imposes a mesh movement for all the points on the hull. This mesh motion is smoothed as before, and the mesh is moved accordingly. The solution for the hull in the previous predicted sunk and trimmed position are used as the initial condition to speed up the steady flow simulation for the hull model at the new position. During subsequent steady flow simulations, the mesh is updated every 100–250 time-steps. This procedure is repeated until convergence of the sinkage and trim is obtained. At most four iterations are required to obtain a converged steady flow solution for a ship free to sink and trim.

5. NUMERICAL RESULTS

The solution algorithm outlined in the preceding sections has been applied to the prediction of sinkage and trim for two hull models at a wide range of Froude numbers (fourteen Froude numbers for each hull model). The wave drag was computed by integrating the pressure over the wetted surface. All simulations were run on a 128-processor R-10000 SGI Origin 2000 in shared-memory mode, using a maximum of eight processors per individual run.

The first case considered is the well-known Wigley hull model defined by the analytical formula:

$$y = \frac{B}{2} \cdot 1 - 4x^2 \cdot \left[1 - \left(\frac{z}{D} \right)^2 \right], \tag{11}$$

where B and D are the nondimensional beam and the draft of the ship at still water. For the case considered here, we have $D = 0.0625$ and $B = 0.1$. A fine triangulation of the surface given by Eq. (11) is first generated. This triangulation is subsequently used to define the hull in a discrete manner. The surface definition of the complete computational domain consists of discrete (hull) and analytical surface patches. The mesh consists of 356,641 tetrahedral elements, 67,395 points and 13,398 boundary points. The free surface has 14,432 triangular elements and 7,445 points. Fourteen Froude numbers, ranging from 0.177 to 0.408, are considered for both model fixed and model free to sink and trim. Figure 3a shows part of the initial surface grids for the Wigley hull model.

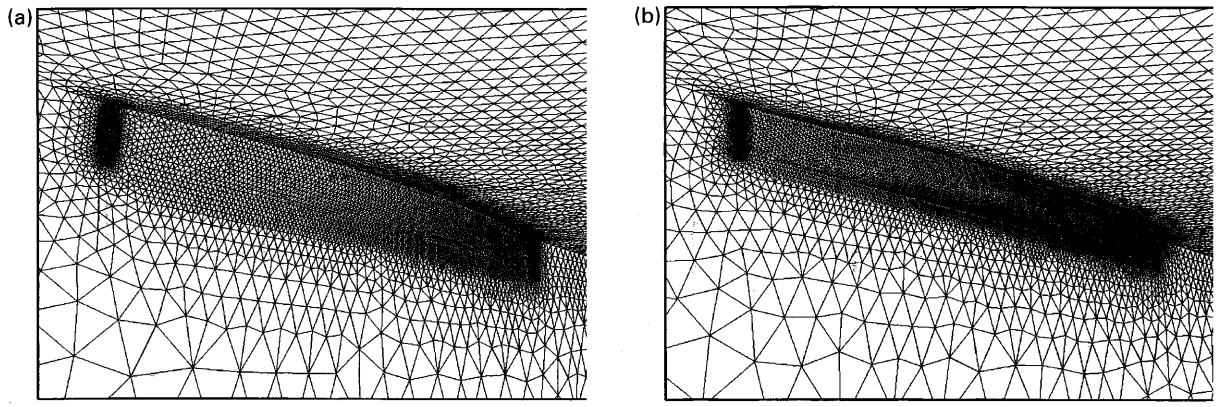

FIGURE 3 (a) Initial surface grids for Wigley hull model. (b) Initial surface grids for Series 60 hull model.

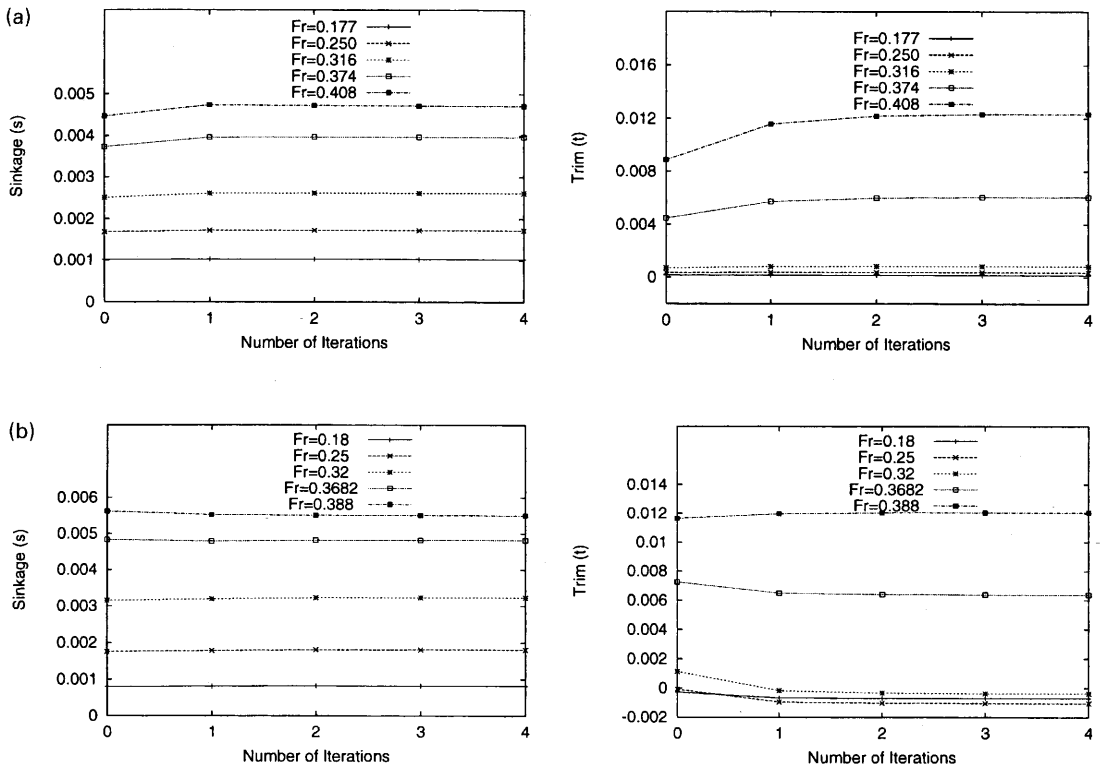

FIGURE 4 (a) Convergence of computed sinkage and trim for Wigley hull model. (b) Convergence of computed sinkage and trim for Series 60 hull model.

The second case considered is the Series 60, $C_b = 0.6$ hull model. A triangulation is first generated from the offset data provided by the DTMB. This triangulation (10,000 triangles) is subsequently used to define the hull in a discrete manner. The surface definition of the complete computational domain consists of discrete (hull) and analytical surface patches. The mesh consists of 343,212 tetrahedral elements, 66,256 points and 16,061 boundary points. The free surface has 15,151 triangular elements and 7,836 points. Fourteen Froude numbers, ranging from 0.18 to 0.388, are considered for both model fixed and model free to sink and trim. Figure 3b shows part of the initial surface grids for the Series 60 hull model.

The computed sinkage s and trim t are defined in accordance with the experimental data as

$$s = (\Delta d_F + \Delta d_A)/L_{pp}, \quad t = (d_A - d_F)/L_{pp},$$

where d_F and d_A are drafts at forward and aft perpendiculars, L_{pp} is the distance between forward and aft perpendiculars, Δd_F and Δd_A are the change of drafts at forward and aft perpendiculars. A positive value of Δd_F or Δd_A corresponds to an increase of the draft from its at-rest position. Therefore, a positive sinkage s is defined as a vertical displacement in the download direction and a positive trim t corresponds to a bow-up rotation.

Numerical results for the Wigley hull model, including sinkage and trim, wave drag coefficient, wave profiles, are compared with the experimental measurements conducted at the University of Tokyo (UT). Numerical results for the Series 60 hull model are compared with the experimental measurements conducted at the UT, Ishikawajima-Harima Heavy Industries (IHHI), and the Ship Research Station of the Korea Institute of Machinery and Metals (SRS).

Figures 4a,b depict the convergence of the computed sinkage h and trim t with respect to the number of iterations for the Wigley hull model and the Series 60 hull model, respectively. Convergence for both models may be seen to be very fast. In practice, two or even one iterations are sufficient. Figures 5a,b, respectively, present a comparison of the computed sinkage and trim for the Wigley hull model and the Series 60 hull model with experimental data. The numerical predictions for both models are in satisfactory agreement with the experimental data for both sinkage and trim. These two figures also show that sinkage and trim are most important at high speed.

Figures 6a,b similarly show a comparison of the computed wave drag coefficient with experimental data for the Wigley hull model and the Series 60 hull model, respectively. The left and right columns of Figs. 6a,b correspond to the fixed and free models, respectively. Numerical predictions are in fair agreement with experimental data. Figure 6c shows the computed wave drag coefficient for the Wigley hull model and the Series 60 hull model fixed and free, respectively. This figure shows that at high Froude numbers (when sinkage and trim are most important) the wave drag is appreciably larger when the model is free to sink and trim.

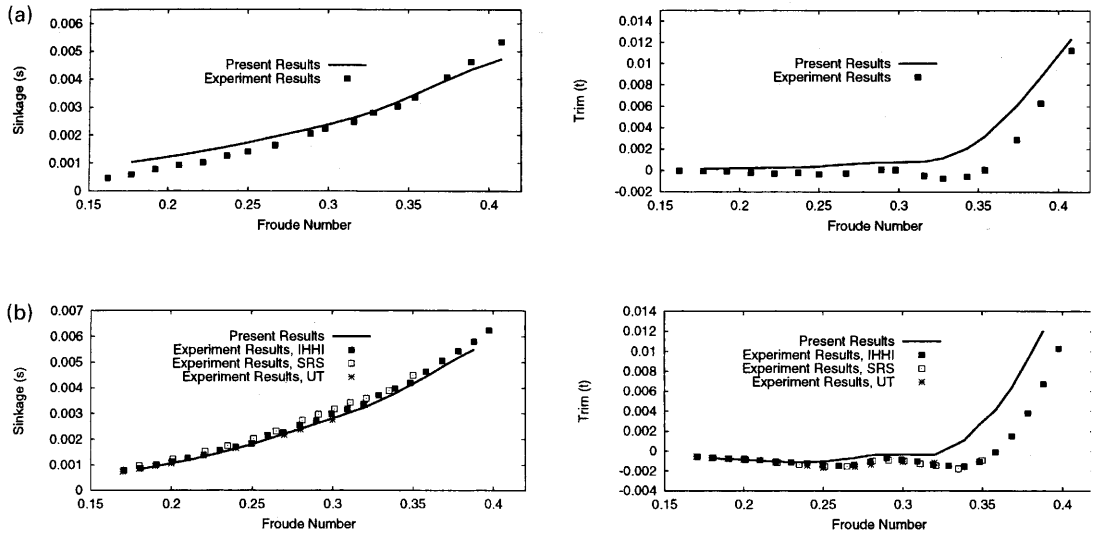

FIGURE 5 (a) Sinkage and trim for Wigley hull model. (b) Sinkage and trim for Series 60 hull model.

The compound wave profiles for the Wigley hull model and the Series 60 hull model are compared with experimental data in Figs. 7a,b, respectively. The left and right columns of these two figures correspond to the models fixed and free to sink and trim, respectively. The computed and experimental wave profiles are in fairly good agreement for both fixed and free models.

Figures 8a,b, respectively, show the computed wave profiles for both ship models fixed and free to sink and trim. The left and right sides of these two figures show the wave profiles measured with respect to the undisturbed water level and the waterline fixed to the hull, respectively. It can be seen that the change of wave elevation (from the fixed to the free to sink and trim condition) with respect to

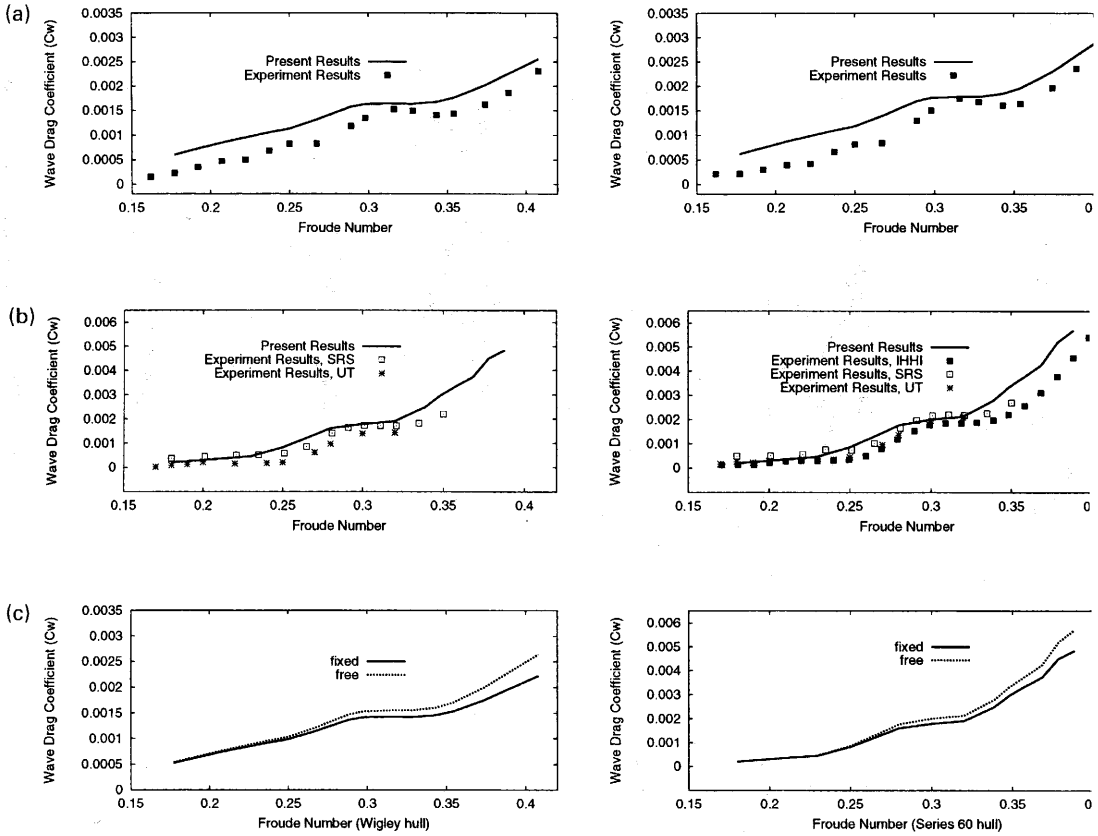

FIGURE 6 (a) Wave drag coefficient for Wigley hull model (left: fixed model, right: free model). (b) Wave drag coefficient for Series 60 hull model (left: fixed model, right: free model). (c) Comparison of wave drag coefficient for fixed and free models.

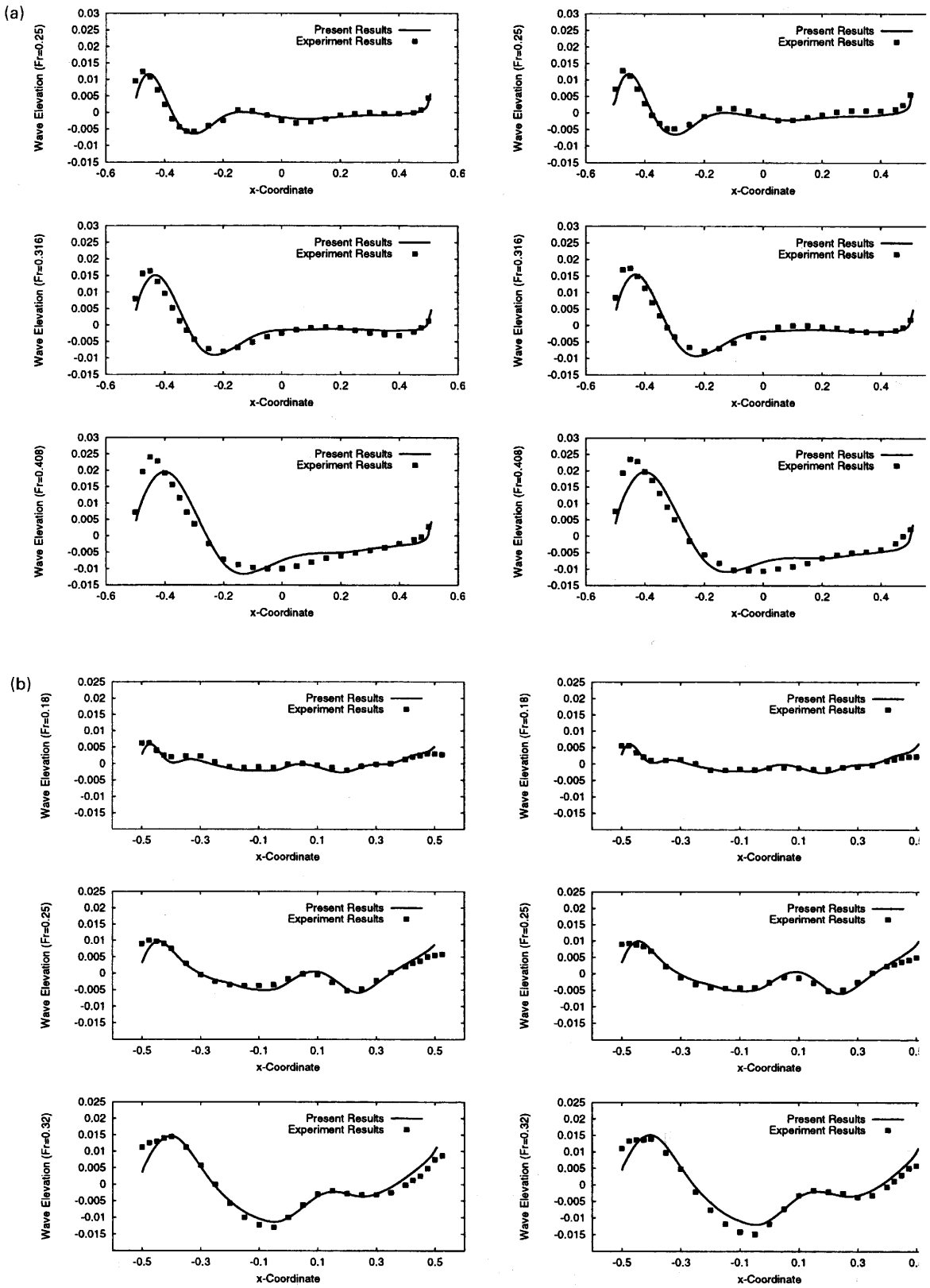

FIGURE 7 (a) Wave profiles for Wigley hull model. (b) Wave profiles for Series 60 hull model.

the still water level is very small. However, if the waterline in the frame fixed to the hull is considered, one can see an increase in the wetted surface for the free to sink and trim condition.

Figures 9a,b show the wave patters for the Wigley hull model and the Series 60 hull model, respectively, in free to sink and trim condition. The wave patterns for each model are plotted using the same contour level for free Froude

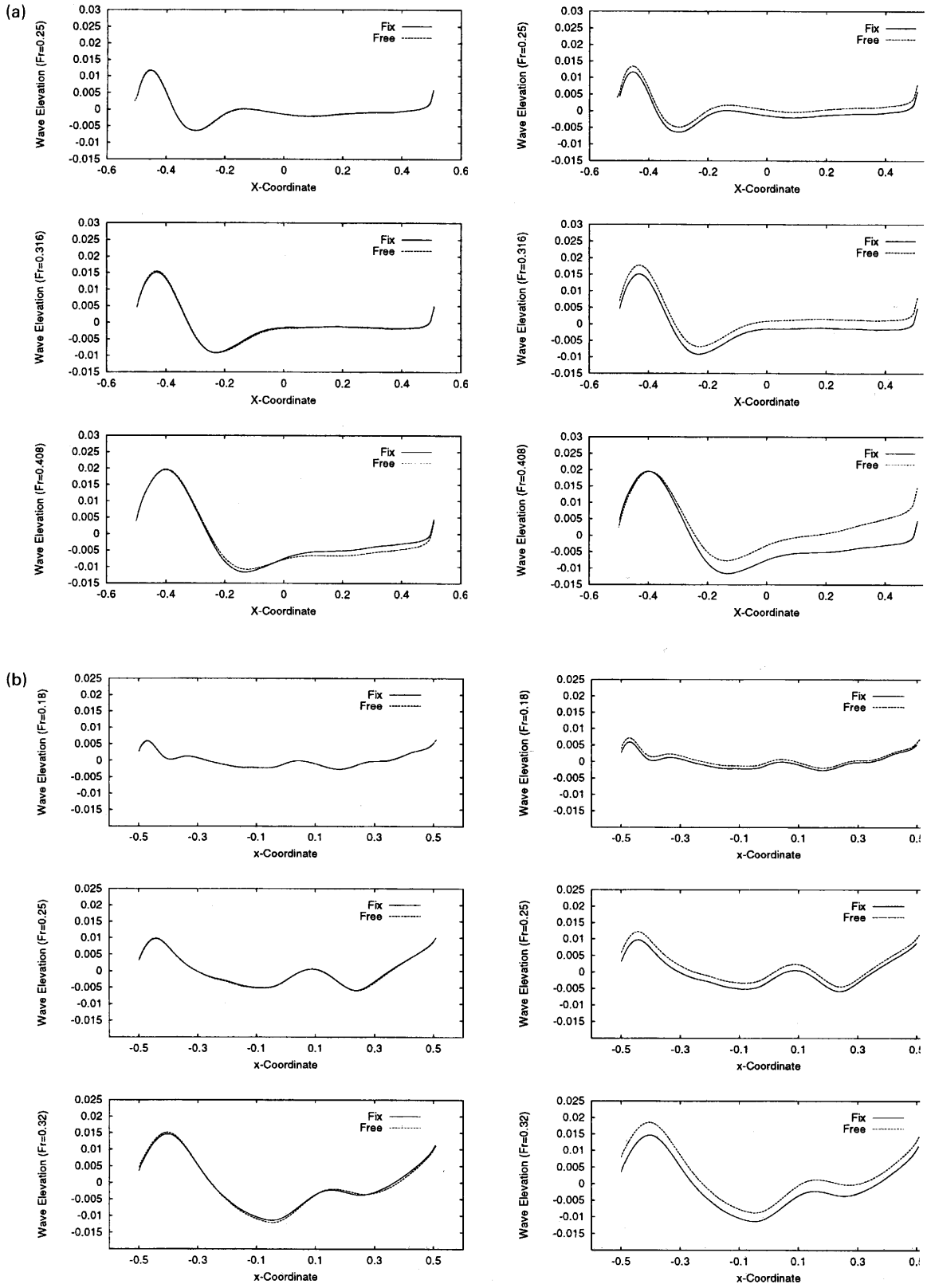

FIGURE 8 (a) Wave profiles for Wigley hull model in fixed and free conditions. (b) Wave profiles for Series 60 hull model in fixed and free conditions.

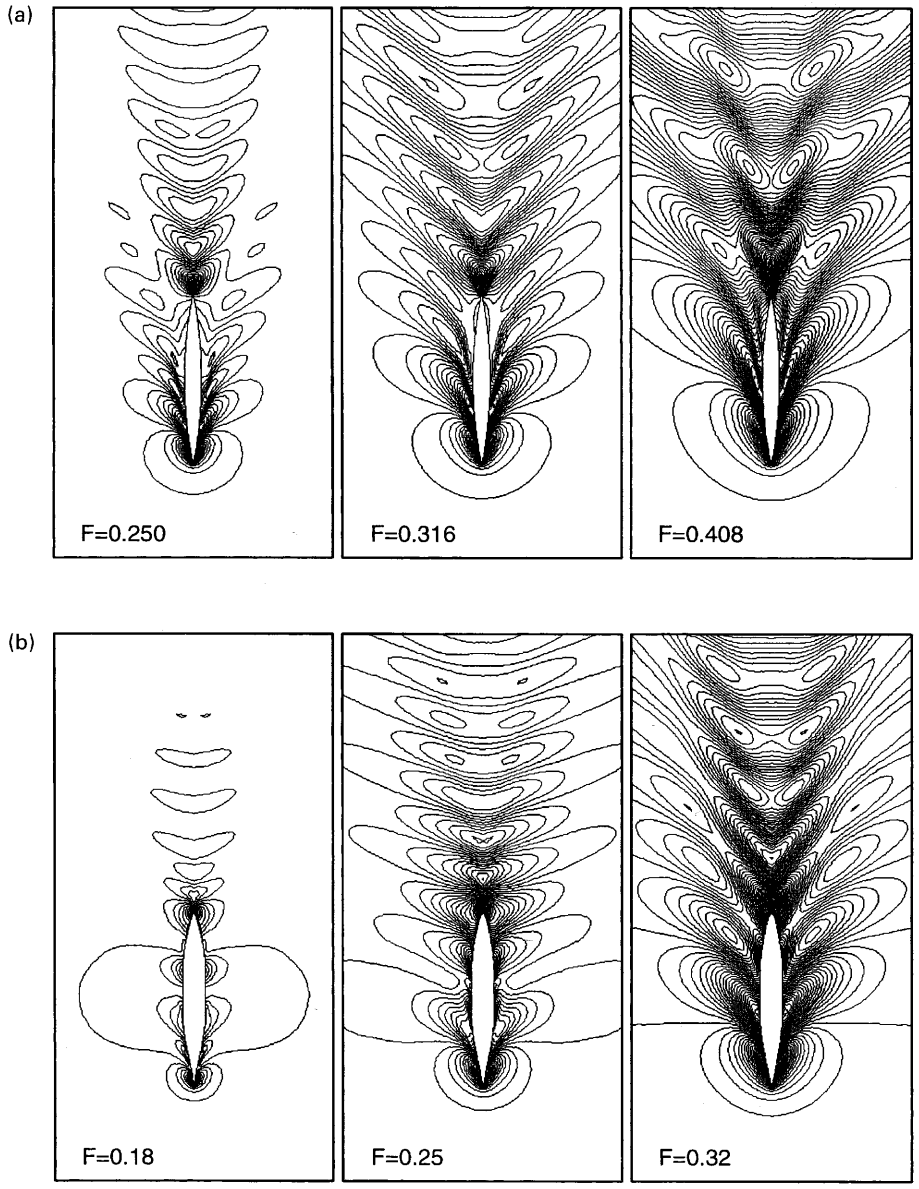

FIGURE 9 (a) Wave patterns for Wigley hull model. (b) Wave patterns for Series 60 hull model.

number considered. These two figures show the change of wave patterns with Froude numbers.

6. CONCLUSIONS

An unstructured grid-based, parallel free-surface solver has been extended to account for sinkage and trim effects in the calculation of steady ship waves. The sinkage and trim, wave profiles, and wave drag computed suing the present approach are in a good agreement with experimental measurements for a mathematical hull form and a practical ship hull form at a wide range of Froude numbers. Our numerical predictions indicate significant differences between the wave drag for a ship model fixed in at-rest position and free to sink and trim, in agreement with experimental observations.

Acknowledgements

This work was partially funded by AFOSR. Dr Leonidas Sakell was the technical monitor. The additional funding was from NRL LCP & FD. Dr William Sandberg was the technical monitor. All runs were performed on a 128-processor R10000 SGI Origin 2000 at the Naval Research Laboratory (NRL).

References

Alessandrini, B., Delhommeau, G., (1996). "A multigrid velocity–pressure-free surface elevation fully coupled solver for calculation of turbulent incompressible flow around a hull." *Proceedings: Twenty-first Symposium on Naval Hydrodynamics*. Trondheim, Norway, June.

Chorin, A.J. (1967) "A numerical solution for solving incompressible viscous flow problems", *J. Comp. Phys.* **2**, 12–26.

Chorin, A.J. (1968) "Numerical solution of the Navier–Stokes equations", *Math. Comp.* **22**, 745–762.

Cowles, G. and Martinelli, L. (1996). "Fully nonlinear hydrodynamic calculations for ship design on parallel computing platforms." *Proceedings*: *Twenty-first Symposium on Naval Hydrodynamics*. Trondheim, Norway, June.

Cowles, G. and Martinelli, L. (1998). "A viscous multiblock flow solver for free-surface calculations on complex geometries." *Proceedings*: *Twenty-second Symposium on Naval Hydrodynamics*. Washington DC, USA.

Farmer, J.R., Martinelli, L. and Jameson, A. (1993) "A fast multigrid method for solving incompressible hydrodynamic problems with free surfaces", *AIAA J.* **6**(32), 1175–1182.

Haussling, H.J. and Miller, R.W. (1994). "Reynolds-Averaged Navier–Stokes computation of free-surface flow about a Series 60 Hull." *Proceedings*: *CFD Tokyo Workshop 1*, Tokyo, Japan.

Haussling, H.J., Miller, R.W. and Coleman, R.M. (1997). "Computation of high-speed turbulent flow about a ship model with a transom stern." *Proceedings*: *The ASME Fluids-Engineering Division Summer Meeting*.

Hino, T. (1989). "Computation of free surface flow around an advancing ship by the Navier–Stokes equation." *Proceedings*: *Fifth International Conference on Numerical Ship Hydrodynamics*. Hiroshima, Japan.

Hino, T. (1997). "An unstructured grid method for incompressible viscous flows with a free surface." AIAA-97-0862.

Hino, T. (1998). "Navier–Stokes computations of ship flows on unstructured grids." *Proceedings*: *Twenty-second Symposium on Naval Hydrodynamics*. Washington DC, USA.

Hino, T., Martinelli, L. and Jameson, A. (1993) "A finite-volume method with unstructured grid for free surface flow", *Proceedings: Sixth International Conference on Numerical Ship Hydrodynamics* (The University of Iowa, Iowa City), Aug.

Kallinderis, Y. and Chen, A. (1996). "An incompressible 3-D Navier–Stokes method with adaptive hybrid grids." AIAA-96-0293.

Kim, J. and Moin, P. (1985) "Application of a fractional-step method to incompressible Navier–Stokes equations", *J. Comp. Phys.* **59**, 308–323.

Löhner, R. (1997) "Automatic unstructured grid generators", *Finite Elements Anal. Des.* **25**, 111–134.

Löhner, R. and Yang, C. (1996) "Improved ALE mesh velocities for moving bodies", *Comm. Num. Meth. Eng.* **12**, 599–608.

Löhner, R., Yang, C. and Oñate, E. (1998). "Viscous free surface hydrodynamics using unstructured grids," *Proceedings*: *Twenty-second symposium on Naval Hydrodynamics*. Washington DC, USA.

Löhner, R., Yang, C., Oñate, E. and Idelssohn, S. (1999) "An unstructured grid-based. Parallel free surface solver", *Appl. Num. Math.* **31**, 271–293.

Luo, H., Baum, J.D. and Löhner, R. (1995). "A finite volume scheme for hydrodynamic free boundary problems on unstructured grids." AIAA-95-0668.

Martin, D. and Löhner, R. (1992). "An implicit linelet-based solver for incompressible flows." AIAA-92-0668.

Martinelli, L. and Farmer, J.R. (1994) "Sailing through the nineties: computational fluid dynamics for ship performance analysis and design", In: Caughey, D.A. and Hafez, M.M., eds, *Frontiers of Computational Fluid Dynamics* (Wiley, New York), Chapter 27.

Miyata, H. (1996). "Time-marching CFD simulation for moving boundary problems." *Proceedings*: *Twenty-first Symposium on Naval Hydrodynamics*. Trondheim, Norway, June.

Peraire, J., Morgan, K. and Peiro, J. (1994) "The simulation of 3D incompressible flows using unstructured grids", In: Caughey, D.A. and Hafez, M.M., eds, *Frontiers of Computational Fluid Dynamics* (Wiley, New York), Chapter 16.

Ramamurti, R. and Löhner, R. (1996) "A parallel implicit incompressible flow solver using unstructured meshes", *Comput. Fluids* **5**, 119–132.

Rizzi, A. and Eriksson, L. (1985) "Computation of inviscid incompressible flow with rotation", *J. Fluid Mech.* **153**, 275–312.

Yang, C. and Löhner, R. (1998). "Fully nonlinear ship wave calculation using unstructured grid and parallel computing." *Proceedings. Third Osaka Colloquium on Advanced CFD Applications to Ship Flow and Hull Form Design*. Osaka, Japan.

Yang, C., Löhner, R., Hendrix, D. and Noblesse, F. (1999). "Fourier-Kochin extension of fully-nonlinear nearfield ship waves." *Proceedings*: *Seventh International Conference on Numerical Ship Hydrodynamics*, Nantes, France.